Simulation of the Performance of a Variable Geometry Turbocharger for Diesel Engine Road Propulsion

G. DESCOMBES[*], J.F. PICHOURON, F. MAROTEAUX, N. MORENO, J. JULLIEN
Université P. et M. Curie
Laboratoire de mécanique physique
2, place de la gare de ceinture
78210 Saint Cyr l'école-France

Abstract

Advanced research work has lead to the development of a new simulation program and the thermodynamic parameters at engine inlet and exhaust of an engine-mounted variable-geometry turbine can thus be evaluated. The machine is divided into characteristic sub-blocks and resolution of thermomechanical flow equations is carried out using the necessary geometrical parameters. A detailed study of losses is conducted experimentally and numerically into the scroll, the vaned nozzle and the rotor in relation to nozzle opening angles. Simulation results made on the variable geometry turbine are analyzed in relation to main flow entry parameters and are compared systematically with experimental data gathered on turbocharger test equipment, and on a Diesel engine used for industrial applications.

Key words: turbocharger variable geometry, turbocharger performance, turbocharger simulation, diesel engine turbocharger

1. Introduction

Turbochargers initially developed with the aim of maximizing engine Power Output and MEP have become an important addition to engines designed with the aim of minimizing emissions. The variable geometry turbocharger, which effectively adapts turbine performance to the thermal engine's varying need for air during partial loads and transient running, is a useful tool to reduce pollution and its effect on public health. The development of a new variable geometry turbine simulation led to a detailed study of energy transformation within each of the characteristic turbine sub-blocks. The objective evaluation of losses in such small machines, where there is often flow blade profile mismatch, is an area for particular concern.

2. Hypothesis

The gas is assumed to be perfect, the flow is compressible, viscous, turbulent, and steady on average, two-dimensional within the volute and quasi 2-D in other turbine sub-blocks. Dividing the turbine into distinct sub-blocks facilitates comparison of results derived from the different models of losses used in the simulation with experimental results. Finally a one-dimensional approach is developed with a reduction of these losses models.

3. Turbine Housing

Distinct configurations of turbine housing were studied, single and double inlet scroll, with smooth and variable geometry bladed distributor (*Figure 1*). The scroll is characterized as a function of azimuth angle θ by the curvature radius $r_c(\theta)$. Trajectory equations $\Gamma(\theta)$ are resolved as a function of curvature radius $r_c(\theta)$ for particular values of θ and $r_c(\theta)$.

3.1. Flow description.

The fluid flow description is made using a two-dimensional approach in the (r,θ) plane, where the observer is placed on the tangential symmetrical axis of the volute, meaning that the three-dimensional effect of the local flow is neglected. Experimental measurements (Frelin 1991) indicate that the flow path can be modeled as a logarithmic spiral (1) and equation (2) indicates the flow incident angle where $\theta > 0$.

---

[*] Author to whom all correspondence should be addressed.

$$r(\theta) = r(0)\exp\big(\theta.tg\alpha(\theta)\big) \tag{1}$$

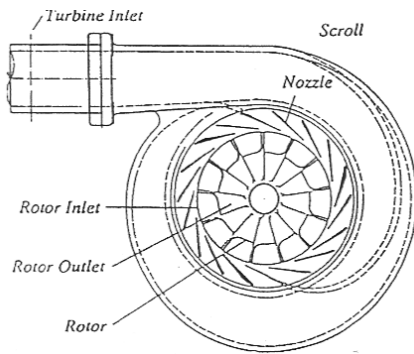$$tg\,\alpha_{is}\big(\theta\big) = \frac{1}{\theta}\,Log\,\frac{r(\theta)}{r(0)} \tag{2}$$

Figure 1. Turbine housing

The complex nature of the flow within the scroll results in losses in quantity of movement and angular momentum and the authors think that these dissipative phenomena share the same origin (Descombes 1997). The flow description is made using 2-D approach according to equations (3) and (4) where r_c is the curvature radius. The terms df_1 and df_2 represent the viscous and swirling losses along the longitudinal and transversal trajectory in the (r, θ) plane.

$$dP + \rho VdV + df_1 = 0 \tag{3}$$

$$dP - \rho V^2 \frac{dr_c}{r_c} - df_2 = 0 \tag{4}$$

3.2. Losses in angular momentum.

Friberg (1985) notes through experimental work that the losses responsible for both trajectory deformation and angular momentum reductions can be approximated respectively by equations (5) and (6) where n is approximately 0.5. Frelin (1991) and Descombes (1997) come to a similar conclusion through 2.5-D numerical experimentation of the flow description in the meridian and circumferential planes on a single inlet turbine with a smooth distributor.

$$tg\alpha(\theta) = tg\,\alpha_{is}(\theta)\left[\frac{r(0)}{r(\theta)}\right]^n \tag{5}$$

$$r^n(\theta)\,V_\theta(\theta) = C^{te} \tag{6}$$

A complementary relation (7) is established in the form of the reduced form of a velocity deceleration coefficient compared with an isentropic angular momentum.

$$\varphi\big(\theta\big) = \frac{V_\theta(\theta)_{real}}{V_{\theta_{is}}(\theta)} = \left[\frac{r(0)}{r(\theta)}\right]^{n-1} \tag{7}$$

A second model is studied by expressing the dissipative terms df_1 and df_2 in the combined equations (3) and (4) as relations 8 and 9. It gives the equation (10) where ξ_f and ξ_D are the respective loss factors along the longitudinal and transverse trajectories (Descombes 1997).

$$df_1 = \zeta_f \frac{\rho}{2} V^2 \frac{dx}{2r} \tag{8}$$

$$df_2 = \zeta_D \frac{\rho}{2} V^2 \frac{dr}{r_c} \tag{9}$$

$$\rho\,V^2 \frac{dr}{r_c}\left[1 + \frac{\zeta_D}{2}\right] + \rho VdV = -\frac{\rho}{2} V^2 d\zeta_f \tag{10}$$

So, the angular momentum can be integrated as equation (11).

$$V_\theta(\theta)\,r(\theta)^{(1+\frac{\zeta_D}{2})} = V_\theta(0)r(0)\exp\left[\frac{-\zeta_f}{2}\right] \tag{11}$$

If we suppose that $\zeta = \zeta_f + \zeta_D$ and with the questionable and simplifying hypothesis that $\zeta_f \cong \zeta_D$, the calculus gives the integrated relation (12) where the loss coefficient $\zeta = \zeta(\theta)$ is thus expressed as a function[4] of azimuth angle θ.

$$r(\theta)\,V_\theta(\theta) = r(0)\,V_\theta(0).$$
$$.\exp\left[\frac{-\zeta}{2}\big|1 + Ln\ r(\theta)\big|\right] \tag{12}$$

3.3. Losses in quantity of movement.

The associated loss coefficient given by equation (13) is expressed as a function of azimuth angle θ (Descombes 1997) and obtained the associated total pressure loss is according to the standard relation (14).

$$\zeta(\theta) = 1 - \varphi(\theta) \tag{13}$$

$$\Delta P_i(\theta) = \frac{\overline{\rho}(\theta)}{2}\,\overline{V}^2(\theta)\zeta(\theta) \tag{14}$$

A complementary expression of pressure loss is derived from equations (3) and (4) of movement (Descombes 1997). Equation (15) integrated according to relation (16) where the loss coefficient is again expressed as a function of azimuth angle θ.

$$-\frac{dr}{r} - \frac{dV}{V} = \frac{\rho}{2} d\big[f_1 + f_2\big] \tag{15}$$

$$\zeta(\theta) = -\frac{2}{\rho} Ln\,\frac{r(\theta)V_\theta(\theta)}{r(0)\,V_\theta(0)} \tag{16}$$

3.4. Simulation results and validation.

Simulation results correspond to steady adiabatic airflow in order to simplify comparisons with experimental data. Thermodynamic parameters of the scroll are established along five distinct streamlines. Thermodynamics conditions at turbine inlet are $P_{ie} = 180$ kPa, $T_{ie} = 973$ K, $q_m = 0.24$ kg/s. *Figure 2* shows the local distribution of the total pressure losses as a function of the azimutal angle in the range $0 < \theta < \pi$. The reduced velocity deceleration coefficient is found to be 0.87 and the total pressure losses 1.4 %. The associated pressure coefficient is approximately 0.1. The results are in accordance with the correlation made by Whitfield (1992) and Baines (1992). The average static enthalpy loss coefficient is 0.06, and converges towards the range suggested by Hribernick et al. (1993). *Figure 3* compares the analytical modeling with experimental data (Fevre 1990) which are in convenient agreement between the distribution of the absolute velocities V and the flow incident angle α in the plane (r, z) where the radius is equal to 36 mm.
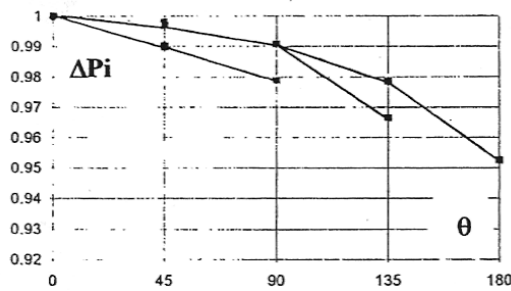
Figure 2. Local distribution of the total pressure losses

The analysis shows also that the maximum standard deflection between the different models (5) to (16) is less than 2.5 %. These results are in agreement with experimental measurements (Strüble et al. 1990). They show that a type of function as $(A/r)^n$ is more appropriate to take into account the losses evolutions.

A 2-D modeling is also conducted with an industrial software on an hybrid mesh within a single scroll with vaneless distributor. The computational solver used an implicit resolution (2nd step) by finite volumes and the turbulent loss models are derived from the k, ε model. The flow conditions at turbine inlet are $P_{ie} = 200$ kPa and $T_{ie} = 500$ K, the exiting static pressure is $P_s = 150$ kPa. *Figure 4* shows the Mach distribution simulated within the scroll which is in agreement with analytical and experimental results from literature. Baskharone (1984) has led a laser experimentation and a 3-D analysis within a

vaned scroll compared with experimentation. He has found a deflection of 2 to 4% of the pressure static distribution on a similar tested point.
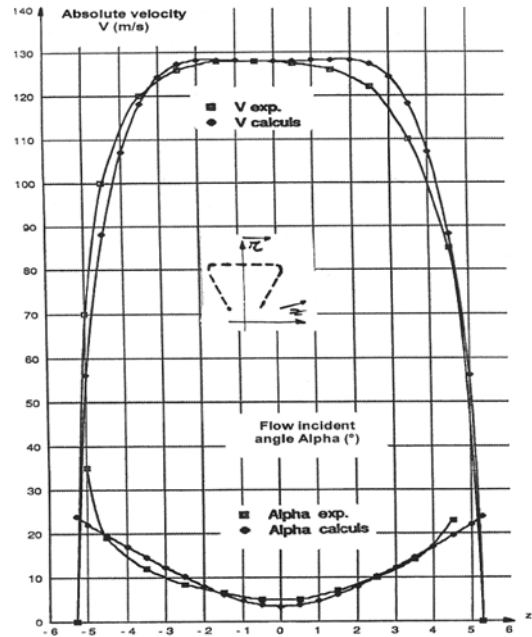
Figure 3. Comparison of modeling and measurements of absolute velocity V and flow incident angle α

Strüble and Benisek (1990) have used a numerical scheme based on the velocity potential function. They note a deflection of 2 to 4% in the computed distribution of the static pressure compared to measurement. We observe that the model results reproduce correctly the description of the vortex flow in the range of $(2\pi - \varepsilon, 2\pi + \varepsilon)$ azimuth teta as *Figure 5* which shows the distribution of the static enthalpy. This region produces an important irreversibility due to the recirculation of a function of the tangential flow, which mixes with the principal flux. Furukawa (1991) observes a leap of the pressure gradient in this zone within a similar scroll.
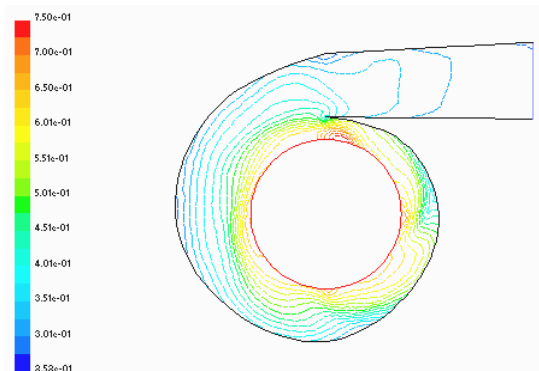
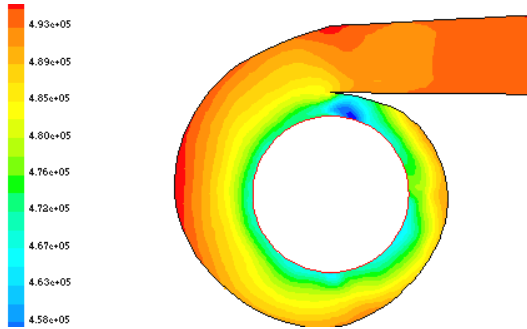*Figure 4. Mach number distribution within the scroll*

Figure 5 Profiles of static enthalpy (kJ/kg) within the scroll

By combining the equations of continuity and conservation of movement, the incident angle α_s between the inlet e and outlet s of the turbine housing can be calculated as a function (17) of global flow conditions at turbine inlet. Hribernick et al. 1993 mention a deflection of 4 to 6% of the flow incident angle at the outlet of the scroll with incompressible calculation. *Figure 6* gives a view of the compressible flow absolute speed contours at the scroll exit radius.

$$tg\alpha_s = \frac{\rho_e}{\rho_s} \cdot A_e \cdot \frac{1}{\theta_s l_s} \cdot r_e^{-n} \cdot r_s^{n-1} \qquad (17)$$
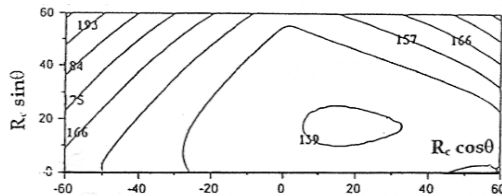

Figure 6. Absolute flow speed contours at scroll exit

4. Variable Geometry Vaned Channel

The inlet to each vaned channel is likened to an isolated wing profile whilst the central channel is modeled by a convergent section identified by its inlet and outlet cross-sectional areas. The outlet periphery of the vaned channels completes the calculation within the distributor. *Figure 7* shows the radial turbine stage and geometrical variables taken into account are the chord length l, blade profile curve radius r_c, blade thickness e, gap between shaft and housing ε_l. At a given point, the inlet profile incident angle α_e and the distance between blades b_e and b_s complete the required geometrical parameters.

4.1. Dissipative phenomena.

Losses by mixing and by flow blade profile mismatch are evaluated by means of models extracted from appropriate articles (Baines 1992, Casartelli et al. 1997) whilst those due to viscous effects, diffusion and compressibility are given in the form of a leap in static enthalpy and

depend upon the exit Mach number, relation (18).

$$\zeta_N = \frac{2 \ (h \ - h_{is})}{V_2^2}\left[1 + \frac{\gamma M_2^2}{2}\right] \qquad (18)$$

The losses by leakage, representing a major handicap to energy transformation, are evaluated by Okazaki (1992). This relation (19) takes into account the deflection α_s at blade exit.

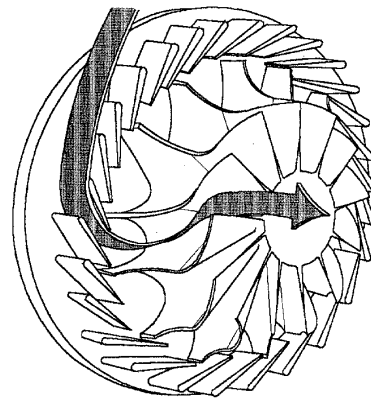$$q_f \cong q_m \frac{\varepsilon_l}{b\sin\alpha_s} \qquad (19)$$

Figure 4. Helicoradial turbine stage

Losses due to an incidence mismatch at the vaned channel outlet are calculated using relation (20) used by Baines (1992) where c is the perpendicular exit throat and b the gap between two blades. This implies that the flow is asymmetric and gives a geometrical rather than a real exit angle.

$$arc\cos\alpha = \frac{c}{b} \qquad (20)$$

For subsonic flow, relation (21) derived from work of Borda-Carnot is employed, and the loss factor τ is a function of the sine of the blade exit angle α_s.

$$\tau = k\left[1 - \frac{A_s}{A_e}\right]^2 \sin\alpha_s \qquad (21)$$

When choking is about to occur, Jansen (1965) and Pluviose (1991) offer an alternative relation for evaluating the losses associated with the supersonic under-expansion in the form of a loss coefficient (22) expressed either side of the shock wave with respect to an ideal transformation.

$$\zeta = 1 - \left[\frac{M_2}{M_{2,is}}\right]^2 \qquad (22)$$

4.2. Resolution schema

A preliminary calculation of the sonic cross-section of the flow at diffuser inlet verifies the compatibility of the currently studied point with the imposed initial fluid flow parameters. Once the flow parameters on the inlet periphery of the smooth distributor are complete, one proceeds to the inlet of the vaned channels, retaining the hypothesis of adiabatic flow. Following this, the calculations are then conducted within the vaned distributor by combining the equations of continuity, conservation of energy and entropy production. This leads to an integrated form (23) where velocity V_{i+1} is the unique unknown term and is resolved numerically. Δi corresponds to the geometrical calculation step within the vaned channels.

$$A_{i+1} V_{i+1}^2 + B_{i+1} V_{i+1}^{1-\gamma} - T_{i_i} = 0 \qquad (23)$$

Coefficients A and B are expressed by (24) and (25), where α_i and α_{i+1} correspond to the respective incidence angles at each calculation point along the mean trajectory within the vaned channel.

$$A_{i+1} = \frac{1}{2Cp} \qquad (24)$$

$$B_{i+1} = T_i \left[\frac{A_i}{A_{i+1}} \right]^{\gamma-1} \left[V_i . \sin(\alpha_i) \right]^{\gamma-1} .$$
$$. \left[\sin \alpha_{i+1} \right]^{1-\gamma} \left[\exp \frac{\Delta S}{r} \right]^{\gamma-1} \qquad (25)$$

4.3. Simulation results and validation

The results presented correspond to a 80% open distributor position. The flow conditions at turbine inlet are $P_{ie} = 250000Pa$, $T_{ie} = 773K$ and mass flow varies in the range of 0.1 to 0.5 kg/s. *Figure 8* indicates the distribution of enthalpy losses within the distributor at this opening position. Over this mass flow range, comparison of simulation with experimental results from Sokhey et al. (1987) seems satisfactory. Leakage losses, assuming a clearance of 0.1 mm, as specified by Spraker (1987) represent only about 1 to 2% of mass flow for this 80% open position. The real incidence angle exiting from the smooth distributor is approximately 40°, in other words 2% higher than the theoretical isentropic value.

Losses due to incidence mismatch represent 30% of total losses for low mass flow rates and fall to around 15% beyond a median flow rate. Losses due to diffusion and compressibility take over beyond Mach 0.5 and evolve as a semi-exponential loss curve which arises due to mixing at distributor exit and is a function of
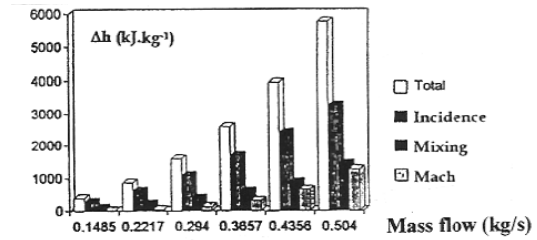

Figure 8. Static enthalpy losses within the vaned channel

flow rate. Comparision with experimental results from Rogo (1987) over this range of flow shows good agreement. *Figure 9* shows the structure of the supersonic jet exiting a channel scale model visualized by strioscopy on a test bench for a pressure ratio of 2:1. *Figure 10* supplies numerical values to the isomach contour lines of the chocked jet for the same ratio pressure. Choking takes place at the channel exit throat accompanied by a marked gradient in Mach number in the exit plane.
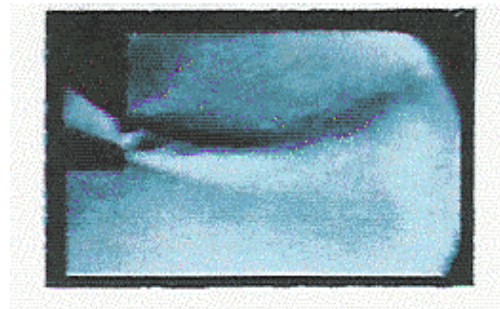

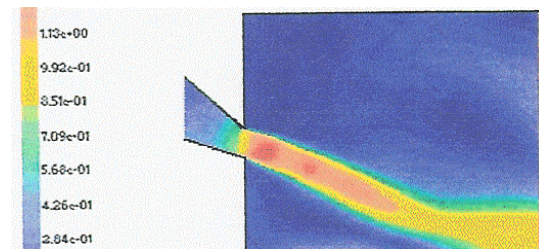*Figure 9. Strioscopic visualization of supersonic expansion*

Figure 10. Isomach modeling of a confined supersonic jet

The total pressure losses show a relative increase of about 10 % for an 80% closed position. This is principally due to more losses through compressibility and sudden flow expansion (Kim et al. 1996). Schölch (1992) makes the same observation experimentally by studying the influence of the blade deflection on distributor performance. Finally, *Figure 11* indicates distributor permeability as a function of its opening position from fully open to fully closed. The closed position corresponds to 20% of the fully open position.
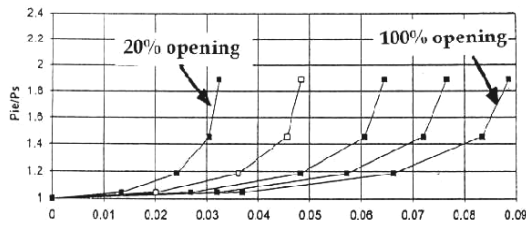
Figure 11. Distributor permeability as a function of its opening position

5. Rotor

The geometry of the radial-inflow rotor is identified by a standard rotor schema. The inlet between blades is characterized by the radius r_1, the gap between blades b_1, the width h_1 and the thickness of blades e_1. The exit is characterized by the outer radius r_2 and r'_2 at respectively the tip and hub of the blades, their respective thicknesses e_2 and e'_2, and the associated blade profile angles β_2 and β'_2 ; ϵ_l and ϵ_h represent respectively the gap in the disk and cover.

5.1. Dissipative phenomena

The losses are calculated by using the same correlation presented in the distributor section. The absolute variables α and V are replaced respectively by relative variables β and W. Experience shows that the power lost by disk friction can be expressed as in (26) where λ_t is a coefficient dependent upon Reynolds number, the ratio e/r and disk roughness.

$$\dot{W} = \pi \omega^3 \lambda_t \rho \frac{1}{5} \left[r^5 - r'^5 \right] \tag{26}$$

Losses by incidence are estimated by a detailed calculation since they represent the main source of losses over wide range of operating speeds and can rise to 80% of all losses within the rotor. All flow parameters are evaluated just before and after rotor inlet and the resulting change in static enthalpy is calculated from local flow conditions. At entry to and relative to the rotor, the blade is at a geometrical angle of $\beta^* = 90°$, and the flow trajectory necessarily satisfies the relation $W = W_m$, a condition imposed by the blade geometry, the relative speed here being equal to the mean speed. The suffix ' refers to conditions just after inlet of the rotor, and enthalpy h' can be evaluated from either relative (27) or rothalpic (28) total enthalpy, both of which remain constant at rotor inlet.

$$h_{iw} = h + \frac{W^2}{2} = h' + \frac{W'^2}{2} \tag{27}$$

$$h' = I - \frac{W'^2}{2} + \frac{U^2}{2} \tag{28}$$

5.2. Resolution schema

A preliminary test is made in order to link mass flow and incidence conditions at distributor exit and rotor inlet. By combining the equations for conservation of quantity of movement and energy, a complete flow description, in absolute and relative terms, can be established, where I and h_i represent respectively the total rothalpic enthalpy and total absolute enthalpy. This description complies with equations (29) and (30), established without restrictions on local entropy production in adiabatic flow.

$$I = h + \frac{W^2}{2} - \frac{U^2}{2} \tag{29}$$

$$h_i = I + UV_\theta \tag{30}$$

Static values remain constant either in absolute or relative terms, and it is thus possible now to evaluate all relative aerodynamic and thermodynamic parameters. The continuity equation, relative to sonic conditions within the bladed channel is expressed by (31), where the subscripts w_1 and w_2 identify the inlet and outlet borders of the rotor in rotational coordinates. A_{*w1} and A_{*w2} represent the associated sonic sections and β_1 and β_2 the incidence angles.

$$A_{*w2} \sin \beta_2 = A_{*w1} \sin \beta_1 \frac{P_{iw2is}}{P_{iw2}} \cdot$$
$$\cdot \left[1 + \frac{U_2^2 - U_1^2}{2C_P T_{iw1}} \right]^{-\frac{\gamma+1}{2(\gamma-1)}} \tag{31}$$

Total relative pressure loss (32) is expressed as a function of the calculated entropy production. The relative efficiency of the energy transformation within the rotor is given by (33), Meauzé (1995).

$$\frac{P_{iw2is}}{P_{iw2}} = \left[\frac{T_{iw2is}}{T_{iw2}} \right]^{\frac{\gamma}{\gamma-1}} \exp \left[\frac{-\Delta S}{r} \right] \tag{32}$$

$$\eta_w = \frac{P_{iw2}}{P_{iw2is}} \tag{33}$$

5.3. Simulation results and validation

Simulation results undergo an entropy analysis over a wide range of turbine operating speeds and for an 80% open position (Descombes et al. 1997). Conditions at turbine inlet are P_{ie} = 250000 Pa, T_{ie} = 773 K, 0.1 < q_m < 0.5 kg/s, corresponding to a flow speed at turbine inlet between 30 and 140 m/s. Losses due to leakage are of the order of 4% for a marked negative incidence mismatch and fall to about 1% for good flow/blade profile fit. *Figure 12* shows losses within the rotor as a function of

relative static enthalpy. *Figure 13* indicates the relative proportions of losses due to incidence mismatch, viscosity and compressibility effects. One notices however that most empirical expressions for flow-profile deviation mentioned in articles are purely geometrical, and fail to take into account changes in mass flow and the associated incidence variations (Matyshok and Stoffel 1997, Ehrlich et al 1997). Hawthorne (1994) suggests expressing the variation of flow-profile deviation by relating the current exit angle β to the sonic angle β* at the throat. This model, often used, requires further study. The simulation results are confirmed by experimental studies led by Lavy et al. (1991) and Connor and Flaxington (1994) for the velocity and pressure radial distribution.
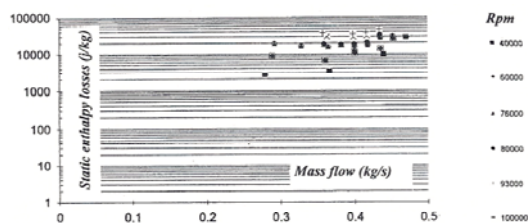

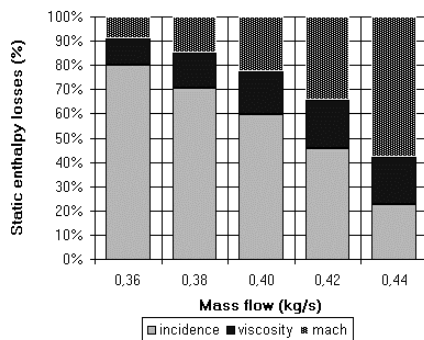*Figure 12. Relative static enthalpy losses within the rotor*

Figure 13. Relative proportions of mean losses within the stage turbine (N=80000 rpm)

6. Turbine

Total pressure and temperature at the variable geometry turbine inlet define the starting parameters. The mass flow through the turbine is a function of static pressure at the exit. The flow calculations validated within each turbine sub-block are conducted once more following the same procedure, and the difference between these and experimental values is measured.

6.1. Trend validation

The behavior of the complete model is compared with available experimental data. Rogo (1987) conducted important experimental work on a small variable geometry gas turbine for which expansion ratios varied over a range

from 2 to 6. The efficiency curve, as a function of flow rate first of all shows no indication of any inflection point for specific iso-regimes of 80% and 60%, and secondly falls between 6% and 20% around the optimum 100% iso-regime. This trend can also be seen for the specific iso-regime 1439 (40000 rpm). Benisek (1994) uses for experimentation a variable geometry helicoradial turbine with curved blades for an expansion ratio over a range from 1.4 to 2.4 and three distinct nozzle positions. One finds again the same trend in simulated results. The validation of such results is completed by comparison with work of Hayashi (1992) and Payri et al. 2000. The envelope of the simulated results is in good agreement with permeability trends stated by the authors.

6.2. Validation on the turbine

Calculated results are compared to the complete experimental variable geometry turbine performance map. The analysis is firstly conducted over the 60000 < N_t (rpm) < 80000 rotor speed range. For the 60000 rpm rotor speed, the error in efficiency values is approximately 5% for expansion ratios in the range 1.25< τ <1.4. The analysis is conducted for a specific experimental rotor speed line, 2769 (77000) which falls between the simulated lines 2734 (76000) and 2877 (80000) for an 80% open distributor position. A measure of errors is done first by comparing the efficiency curves as a function of expansion ratio. *Figure 14* shows that the 2734 (76000) model speed profile is very similar to the experimental 2769 (77000) profile. Simulation results cover a widened expansion ratio envelope 1.2< τ <1.9 compared to experimental values, for which 1.4< τ <1.65. The average difference remains less than 3%, whilst the maximum difference is around 6%.
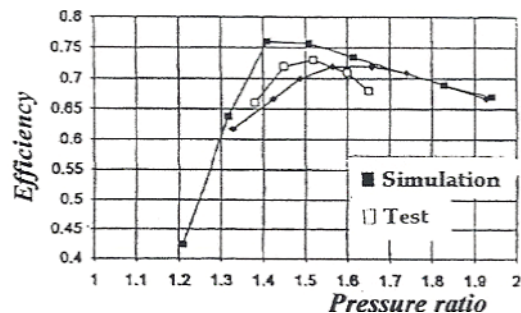

Figure 14. Expansion ratio model and experimental efficiency values

One notes, unsurprisingly a small translation of the efficiency curve for the 2877 (80000) curve, as a function of expansion ratio. One also notes however a deviation of specific mass flow rate, the simulation giving values 6% higher, with respect to the point considered. The gap between the two sets of results can be

explained by the difference in turbine sizes. Whilst both machines comprise a variable geometry distributor, the turbine studied is intended for use on an 11-liter Diesel engine turbocharger and the experimental measurements were made on a 10-liter Diesel engine. It seems necessary therefore to establish a correlation to link and provide a better comparision of the two sets of results. Scaling laws are a means of comparing the performance of similarly shaped by differently sized machines using the fluid flow velocity triangles. For identical turbine inlet pressure and temperature conditions, the similarity laws indicate that the thermodynamic distribution is, in principle the same. Equations (34) and (35) can thus be deduced, noting beforehand the equality of (36). Equation (37) is formed by considering the conservation of velocity triangles, which govern the mechanical work recuperated on the shaft.

$$U = \frac{N\pi 2r}{60} = C^{te} \tag{34}$$

$$Nr = C^{te} \tag{35}$$

$$\frac{q_m}{r^2} = C^{te} \tag{36}$$

$$\frac{W}{r^2} = C^{te} \tag{37}$$

In this way, for similar machinery for which the dimensions are multiplied by a factor k and through which the same fluid flows following the same flow field, the rotation speeds are divided by factor k, whereas mass and energy flow are multiplied by k². The scaling factor k is evaluated by comparing mass flow rates for engine rotation speeds in the range 800-2000 rpm and the value k=1.062 is concluded and verified.

6.3. Validation on the engine.

Validation is completed by comparison with experimental results measured for a stable engine regime on a 10 l Diesel engine at full load (Younès 1993). The fluid description is completed at inlet and outlet to the turbocharger as in *Figure 15* where suffixes 1, 2, 3 and 4 refer to the entry and exit to compressor and turbine.

Known flow conditions upstream of the turbocharger include the pressure, temperature and mass flow rate. Conditions downstream of the turbocharger are governed by the downstream exhaust circuit where pressure loss is given as in (38) where b is evaluated from experimental backpressure established at engine exhaust.
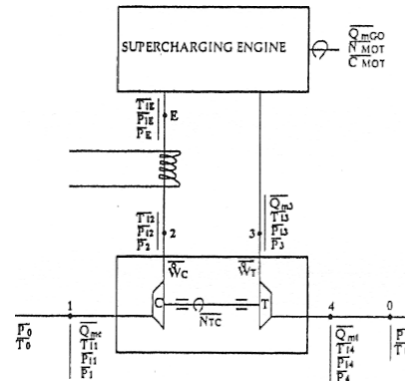
$$\Delta P = b q_m^2 \tag{38}$$

Figure 15. Turbocharging system diagram

Specific mass flow rate is evaluated at turbo inlet and since the total to static expansion ratio is known, the current running point can be situated on the characteristic curve $\tau = \tau(q_m)$, *Figure 16*. This is a unique point which provides firstly the associated specific isospeed and then eases the evaluation of the corresponding efficiency as a function of expansion ratio. The error in total temperature ΔT_i is derived from relation (39). Given the turbine power output (40), the total temperature at outlet T_{i4} is also known (41).
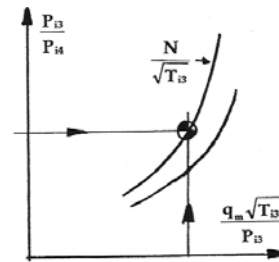

Figure 16. Current running point on the turbine map

$$\eta_s = \frac{\Delta T_i}{T_{i3}\left[1 - \tau_s^{-\frac{\gamma-1}{\gamma}}\right]} \tag{39}$$

$$\dot{W}_T = q_m C_p \Delta T_{iT} \tag{40}$$

$$\Delta T_{iT} = T_{i3} - T_{i4} \tag{41}$$

The rotation speed N_c of the compressor is identical to that of the turbine N_t (42), and mass flows are also considered identical if no information is known at this stage about engine fuel consumption. Power supplied to the compressor (43) is governed by the mechanical efficiency of the turbine shaft.

$$N_C = N_T \tag{42}$$

$$\dot{W}_C = \eta_m \dot{W}_T \tag{43}$$

The power absorbed by bearings and lubrication friction can be evaluated by (44)

which is derived directly from standard equations regarding the design and development of cylindrical oil bearings for rotary machinery. μ is the oil dynamic viscosity, U the peripheral shaft speed, B the length of the bearing and d its diameter. 'a' represents the minimum space where F_f is the bearing friction.

$$\overset{\circ}{W} = \mu \frac{U^2}{a} \pi \, B \, d = F_f \, U \qquad (44)$$

The corresponding running point can thus be situated on the compressor performance chart (*Figure 17*). The compression rate and efficiency are deduced and equations (45) and (46) establish the exit temperature T_{i2}. All flow conditions are thus known at the inlet and outlet ducts to the turbocharger.
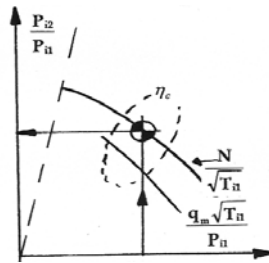

Figure 17. Current running point on the compressor chart

$$\frac{P_{i2}}{P_{i1}} = \left[1 + \eta_C \frac{\Delta T_C}{T_{i1}} \right]^{\frac{\gamma}{\gamma - 1}} \qquad (45)$$

$$\overset{.}{W}_c = q_m C_{pc} \Delta T_i \qquad (46)$$

The simulation is equally tested directly on several engine trial points by systematically recalculating the turbine running point to the response at compressor exit. For known turbine inlet conditions P_{i3} and T_{i3}, the simulated shaft speed and turbine exit temperature are compared with the experimental values. Comparision of simulated and experimental pressure and temperature values at compressor exit complete the tests. The calculations are conducted for fixed engine speeds firstly at low engine speeds and then for maximum torque, and then at full load with different distributor positions. Errors between calculated and experimental values at 800 and 1400 rpm show a suitable convergence of exit temperatures at turbine [Δ<4%] and compressor [Δ<6%]. A deviation appears however in compression rate and is yet to be explained. The validated turbine performance map is established in expansion ratio and efficiency as a function of specific mass flow rate for a mean distributor position. One notes that efficiency systematically falls off once out

of the limited adapted running range. The efficiency as a function of specific flow rate is in accordance with experimental observation made by Parois (1992) who states that the objective of the designer is to dimension the distributor for highest efficiency in the 1000 to 1400 rpm engine running range, and to try and maintain efficiency above 0.5 at other running speeds.

7. Conclusion

The description of energy transformation and associated losses within each sub-block of a variable geometry turbine is presented and systematic verifications have been made. The simulation enables one to establish all parameters and the complete performance at inlet and exit of the machine. Simulation results are compared with experimental results and show an average error of between 4 and 6% for turbine efficiency as a function of expansion ratio. Incidence losses at rotor inlet are the main source of losses. This is quite understandable since the flow angle varies over 100° following the running point considered.

It would be of great use now to make more tests, particularly around the maximum torque engine running point as well as for partial loads. The simulation also requires completion with a model of heat losses in order to take into account the real non-adiabatic environment of the turbine, of particular importance at partial load and low running speeds, which is often the case during urban driving. It would be interesting to take into account the varying gas specific heat as a function of air-fuel ratio and temperature levels. The effect of pulsating flow on the variable geometry turbine performance could also be considered by a preliminary look at the perturbation caused at turbine entry at low engine running speeds.

Nomenclature

θ   azimuth angle
β   rotor blade inlet angle geometry
β'   rotor blade exit angle geometry
Γ   Trajectory
ζ   Factor loss
V   Absolute velocity
W   Relative velocity
U   Speed velocity
r   radius
N_T speed turbine
q_m mass flow
A   Normal area
P   Pressure
T   temperature
h   enthalpy
M   Mach number
I   rothalpy

S   entropy
Z   blade number
e   Blade thickness

Subscripts

c   curvature
i   total values
w   relative coordinates

References

Baines, N. C., 1992, "Introduction to radial turbine technology", Von Karman institute for Fluid dynamics, Lecture Series 1992-05.

Benisek, E., 1994, "Comparisons of laser measurements and pneumatic measurements in a turbocharger turbine", *Institution of Mechanical Engineers* C484/018.

Casartelli, E., Saxer, A.P. and Gyarmathy, G., 1997, "Numerical flow analysis in a subsonic vaned radial diffuser with leading edge redesign", *Asme Paper* 1997.

Connor, W.A. and Flaxington, 1994, "A one dimensional performance prediction method for radial inflow turbine", *Institution of mechanical engineers*, 1994, C405/017.

Descombes, G., Duan, Q., Jullien, J., Parkinson, N., 1998, "Study of the performance of a variable geometry turbocharger", 22nd CIMAC, session no. 0.08, Copenhaguen, may 1998.

Descombes, G., 1997, *Contribution à l'étude des performances d'une turbine de suralimentation à géométrie variable*, Doctoral thesis of University of Paris VI, 1997.

Descombes, G., Duan, Q., Jullien, J., Bois, G.,1997, "Simulation des performances d'une turbine hélicoradiale de suralimentation, Problèmes multidisciplinaires dans les turbomachines", *Journées Société française de mécanique*, 12.1997.

Ehrlich, D., Lawless, B. and Fleeter, S., 1997, "Particle image velocimetry characterisation of a turbocharger turbine inlet flow", *SAE Paper* 970343.

Fèvre, S., 1990, *Application de la vélocimétrie Laser döppler à des mesures de vitesses dans une petite turbine de suralimentation*, Ph. D., Doctoral thesis of University P. and Marie Curie, 1990.

Frelin, M., 1991, *Prévision des caractéristiques d'une turbine radiale à partir des données géométriques*, Ph. D., University P. and M. Curie, 1991.

Friberg, J., 1985, "Particularités des turbocompresseurs d'automobiles", *Revue Française de Mécanique* 1985-3.

Furukawa, M., 1991, "Out flow Boundary conditions for Euler analysis of flow in turbine scroll", FED, Vol 120, Numerical Simulations in Turbomachinery, *Asme* 1991.

Hawthorne, W.R., 1994, "Aspects of the characteristics of radial flow turbines", *Institution of Mechanical engineers* C 484/004 1994.

Hayashi, M., 1992, "Development of a turbocharger system with variable area turbine nozzle for heavy duty trucks", *SAE Paper* 92 0045.

Hribernick, A., Dobovisek, Z., Cernej, A. and Jankowski, A., 1993, "Contribution to determination of boundary conditions at the entrance of a turbocharger twin turbine", Cimac 1993 London- D79.

Jansen, W. & Smith, J.E., 1965, "Supersonic expansion in radial inflow turbine nozzle vanes". *Asme* 65 WA GT P5.

Kim, H.S., Lee, J.S. and Kang, S.H., 1996, "Secondary flow effect on turbulence structure of a flat plate wake", *International Asme Congress on Fluid dynamics and Propulsion*, Le Caire, 12-1996.

Lavy, J., Duan, Q., Jullien, J., Bois, G., 1991, "Mesure des caractéristiques de fonctionnement de turbines de turbo compresseurs en régimes stationnaire et pulse", *Revue française de mécanique*, 1991-3.

Matyshok, B. and Stoffel, B., 1997, "Experimental investigations of the flow at the rotor outlet of a turbocharger turbine", 2nd European conference on turbomachineery fluid dynamics and thermodynamics, Antwerpen, March 5-7, 1997.

Meauzé, G., 1995, "Calcul des écoulements compressibles dans les turbomachines, Collection Techniques de l'Ingénieur", *Traité mécanique et chaleur*, Vol B4, B4181-95.

Okazaki, Y. , 1992, "Development of variable area radial turbine for small turbo chargers", *Asme* Paper GT 92.

Parois, A., 1992, "Turbine à puissance variable pour turbocompresseurs d'automobiles", Conférence Sia-clésia 1992.

Payri, F., Galindo, J., Serrano, J.R, 2000, "Variable geometry turbine modeling and control for turbocharged diesel engine transient operation", Thiesel 2000, International congress on Thermofluidynamic processes in Diesel engines, Valencia, September 2000.

Pluviose, M., 1991, "Instabilities of flow in sudden enlargement", *Asme* Fed, Vol. 128, Experimental and numerical flow visualisation H00 706 1991.

Rodgers, C., 1997, "Turbochargers to small gas turbines", *Asme* Paper 97-GT-200.

Rogo, C., 1987, "Variable stator radial turbine", Contract Nasa 23163, Nasa CR 174663, 1987.

Schölch, M., 1992, "Aerodynamic design of pivotable nozzle vanes for radial inflow turbines", *Asme* Paper 92GT94.

Sokhey, J., Tabakoff, W. and Hosny, J., 1987, "Flow behavior in inlet guide vanes of radial turbines", Nasa CR 137632.

Spraker, N., 1987, "Contour clearance loss in radial inflow turbines for turbocharger", *Asme* Paper 87ICE52.

Strüble, A. G. and Benisek, E. F., 1990, "Flow measurements and flow predictions at the inlet of a turbocharger turbine", *SAE Paper* 900358.

Whitfield, A., 1992, *Non dimensional conceptual design of radial inflow turbines*, Von Karman institute for Fluid Dynamics Lecture Series 1992-05.

Younès, R., 1993, *Elaboration d'un modèle de connaissance d'un moteur Diesel avec turbocompresseur à géométrie variable en vue de l'optimisation de ses émissions*, Doctoral thesis of Ecole Centrale de Lyon, 1993.